Incomplete spin reorientation in yttrium orthoferrite

J. Scola, Y. Dumont, and N. Keller
Groupe d'Étude de la Matière Condensée (GEMaC), UMR 8635 du CNRS, UVSQ, 45 Avenue des États-Unis, 78035 Versailles Cedex, France

M. Vallée and J.-G. Caputo
INSA de Rouen, Math Laboratory, 76801 Saint-Étienne-du-Rouvray, France

I. Sheikin
Grenoble High Magnetic Field Laboratory, UPR 3228 du CNRS, 38042 Grenoble Cedex 9, France

P. Lejay
Institut Néel, CNRS and Université Joseph Fourier, Grenoble, France

A. Pautrat
Laboratoire CRISMAT, UMR 6508 du CNRS, ENSICAEN et Université de Caen, 6 Bd. Maréchal Juin, 14050 Caen, France
(Received 30 November 2010; revised manuscript received 29 March 2011; published 15 September 2011)

High-magnetic-field measurements of the magnetic moment of single crystals of yttrium orthoferrite were performed by torque and vibrating sample magnetometers. We investigated the magnetic states before and at the end of the field-induced spin reorientation and compared them with the theoretical predictions given by a macrospin model. The model describes the spin reorientation for low magnetic fields well. For high magnetic fields, the model predicts a 90° spin rotation while the experiments indicate that the magnetic moment only rotates by 80° for $H = 74$ kOe and remains about 10° out of a crystallographic axis, up to the highest measured field (280 kOe). This suggests that the initial magnetic interactions are altered by the strain induced by the spin reorientation, leading to a symmetry change.

DOI: 10.1103/PhysRevB.84.104429 PACS number(s): 75.30.Gw, 75.47.Lx, 75.50.Ee, 75.40.Mg

I. INTRODUCTION

Rare-earth orthoferrites have a distorted perovskite structure (space group D2h-16-Pbnm). Their low symmetry combined with spin-orbit coupling gives rise to antisymmetric exchange interactions as described by Dzyaloshinsky and Moriya (DM),[1–3] in addition to the antiferromagnetic (AFM) exchange interaction. The DM interaction is responsible for the canting angle (a few milliradians) between the two AFM sublattices and makes the compound a weak ferromagnet. For all rare-earth metals except lanthanum and yttrium, the net magnetization rotates by 90° as the temperature varies between two characteristic temperatures; within this temperature range, the equilibrium magnetization can be found in any direction in the plane (010). This phenomenon, referred to as spin reorientation (SR), has been extensively studied in different orthoferrites (see Ref. 4 for an exhaustive review and Refs. 5 and 6 for more recent studies). SR was initially considered to be the consequence of a crystallographic phase transition, but it eventually turned out to be a purely magnetic phase transition.[5,7] Owing to the very strong magnetic anisotropy of orthoferrites, the rotation of the magnetization induces a strain on the ionic lattice. Investigations of such changes are complicated by the phononic thermal expansion that is mixed with the magnetostriction during the SR. This difficulty can be overcome by inducing the SR by a magnetic field. As a field of tens of kilo-oersteds is applied along the AFM axis (i.e., perpendicular to the weak ferromagnetic moment), the spin structure undergoes a 90° rotation in such a way that the weak ferromagnetic moment aligns with the applied field.[8,9] The field-induced SR at a fixed temperature was studied by neutron diffraction by Koehler *et al*. on $ErFeO_3$ and $HoFeO_3$ up to 10 kOe.[10] Their results suggest structural domain transformations during the SR, but many details were lost because they studied powders. The problem can be simplified further by studying yttrium orthoferrite [$YFeO_3$, $T_N = 648$ K (Ref. 3)]. The Y sites are not magnetic, so the magnetic description of the SR is limited to the iron lattice.

Here we focus our investigations on the magnetic states before and after the SR by vectorial magnetization experiments performed on $YFeO_3$ single crystals (Sec. II). By combining a torque magnetometer and vibrating sample magnetometer (VSM), we monitor the relative direction of the magnetic moment of $YFeO_3$ during the SR. Particular attention is given to the magnetic state at very high fields where the SR is assumed to be completed (Sec. III). Then we compare our observations to a macrospin model using the commonly used magnetic interactions for orthoferrites (Sec. IV). The numerical simulations of the Landau-Lifshitz equations were performed by a relaxation method. In Sec. V, we discuss the discrepancies between the experiments and the model.

II. SAMPLE AND EXPERIMENTS

A. Bulk single crystal

A bulk single crystal was grown using the floating zone technique in a mirror furnace under air at ambient pressure. We used the very high quality precursors Y_2O_3 5*N* and Fe_2O_3 4*N*8. The single crystalline seed was tied with pure platinum wire and the crystal had no contact with any holder during the growth, which rules out any pollution during the

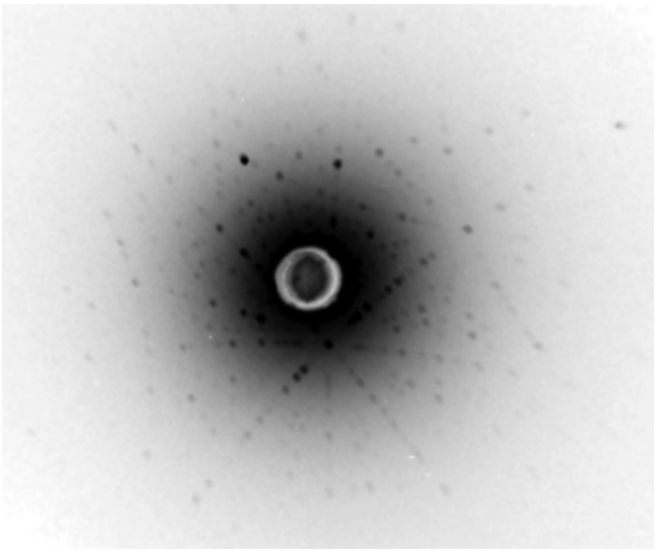

FIG. 1. Laue picture of the $YFeO_3$ single crystal.

growth. Analysis by a scanning electron microscope with a field effect gun reveals that the only elements detected were Y, Fe, and O in the appropriate concentrations; no parasitic compounds were detected. This was confirmed by the x-ray powder diffraction measurements carried out on crushed single crystal mixed with pure silicon as standard. In the bulk, the refined lattice constants were $a = 5.2818$ Å, $b = 5.5953$ Å, and $c = 7.6054$ Å. The mosaicity was estimated from a Laue picture to be less than 0.5° (Fig. 1) The crystal was cut along the crystallographic faces into a $1.90 \times 1.96 \times 1.99$ mm^3 cube and a $200 \times 100 \times 40$ μm^3 nearly cuboid sample for the vibrating sample magnetometer (VSM) and torque magnetometer, respectively.

B. Experiments

Torque magnetometry informs on the magnetization vector and offers a very good resolution even at high field. The samples were rigidly glued on 125-μm-thick CuBe cantilevers. The small deflections of the cantilever caused by the magnetic torque $\mathbf{T} = \mathbf{m} \times \mathbf{H}$ ($\mathbf{m}$ being the magnetic moment of the sample and $\mathbf{H}$ the applied field) were detected by a high-resolution capacitance bridge. In the experimental configuration, the output signal is the x component of $\mathbf{T}$ as schematically represented in Fig. 2. Magnetization measurements were performed in 9-T and 14-T Quantum Design VSM's.

III. EXPERIMENTAL RESULTS

A. Magnetization

Figure 3 presents the magnetization of the $YFeO_3$ single crystal for $\mathbf{H}$ applied along $\mathbf{a}$ and $\mathbf{c}$ at $T = 4.2$ K. We duplicated the Jacobs *et al.* experiment[9] on a single crystal grown from state-of-the-art precursor purity. Comparisons with the previous results are summarized in Table I. In contrast with the literature (e.g., Refs. 9 and 11), we observe that the magnetization remains smaller for $\mathbf{H}\|\mathbf{a}$ than for $\mathbf{H}\|\mathbf{c}$ even for high fields after the spin reorientation. This difference can be due to either a smaller net magnetization or a finite angle

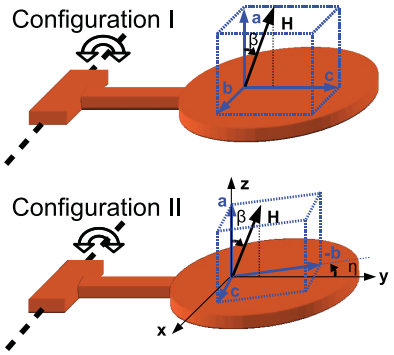

FIG. 2. (Color online) Experimental geometry for torque magnetometry measurements. Relative orientations of the sample crystallographic axes ($\mathbf{a}$,$\mathbf{b}$,$\mathbf{c}$) and the reference system of coordinates ($\mathbf{e_x}$,$\mathbf{e_y}$,$\mathbf{e_z}$) are given for the two experimental configurations. The deflection of the cantilever is symbolized by the curved arrow. In this drawing, $\beta > 0$ and $\eta > 0$.

between the magnetic moment and the applied field. The torque experiment will confirm the second explanation.

B. Torque magnetometry

We used a torque magnetometer in order to study the magnetic moment direction at high field at room temperature. The SR was probed in two distinct experimental configurations, sketched in Fig. 2 and referred to as configurations I and II; ($\mathbf{e_x}$,$\mathbf{e_y}$,$\mathbf{e_z}$) represents the reference system of coordinates. In configuration I, the output signal is proportional to

$$\frac{T_x}{H} = \cos(\beta) m_c(\mathbf{H}) - \sin(\beta) m_a(\mathbf{H}), \qquad (1)$$

where $\mathbf{H} = H(\cos\beta \mathbf{e_z} + \sin\beta \mathbf{e_x})$. In our convention and for $H > 0$, m_c is positive (negative) for β positive (negative) while m_a is positive for all β.

The torque was measured continuously while the magnetic field was swept up and down and is presented in Fig. 4. The angle $\beta = 6°$ was obtained from the results of Fig. 5

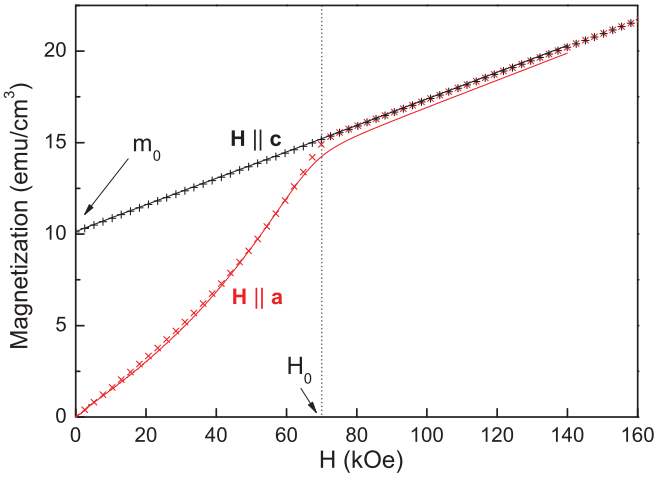

FIG. 3. (Color online) Solid lines indicate magnetization measured for two orientations of the magnetic field. + and × symbols are numerical simulations. Arrows indicate quantities discussed in the text. $T = 4.2$ K.

TABLE I. Summary of the experimental data and the deduced interaction fields in $YFeO_3$. M_0 is given in 10^{-5} emu/cm^3 and χ in 10^{-4} emu/kOe. Also presented are the interaction fields obtained in Ref. 9 at $T = 4.2$ K.

	$T = 4.2$ K	$T = 300$ K	Ref. 9
M_0	7.51	6.6	
χ	5.38	5.79	
H_0 (kOe)	70.0	74.3	74
ϕ_0 (mrad)	12.3		10.9
H_D (kOe)	140	140	140
H_E (kOe)	5700	5300	6400
H_2 (kOe)	1.3	1.3	1.2
H_4 (kOe)	0.50	0.44	0.52

as described below. The quantity T_x/H takes its maximum value at low fields and decreases with increasing field. The angle between **H** and **m** is initially 90° and tends to decrease during the SR. As the field is applied, the magnetic moment **m** rotates from **c** for $\beta > 0$ ($-$**c** for $\beta < 0$) toward **a**.

In configuration II, the output signal is proportional to

$$\frac{T_x}{H} = -\cos\eta\cos\beta m_b(\mathbf{H}) + \sin\eta\cos\beta m_c(\mathbf{H}) - \sin\beta m_a(\mathbf{H}), \quad (2)$$

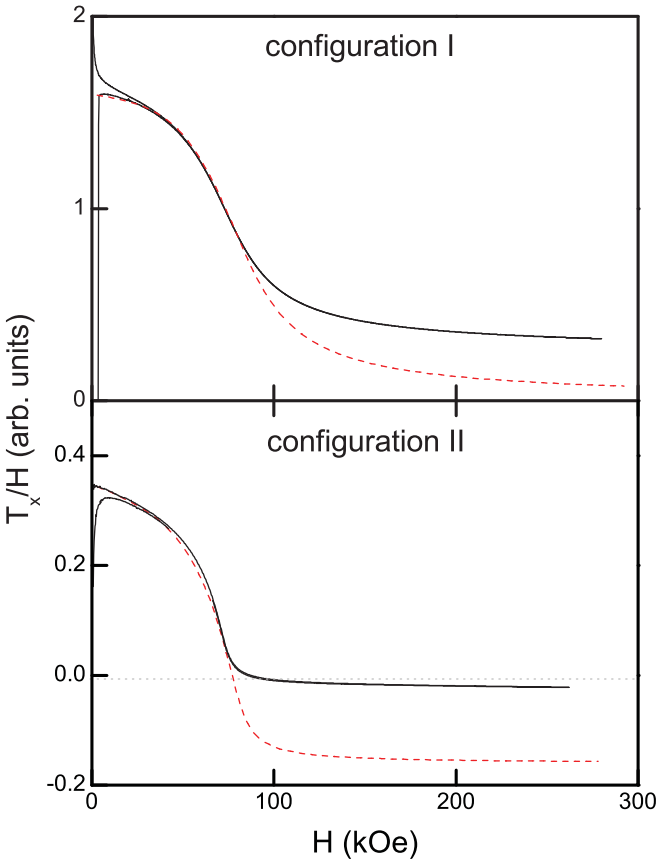

FIG. 4. (Color online) Experimental (solid line) and simulated (dashed line) torque signal T_x/H for experimental configuration I (upper panel) and configuration II (lower panel). $\beta = 6°$, $\eta = 12°$, $T = 300$ K.

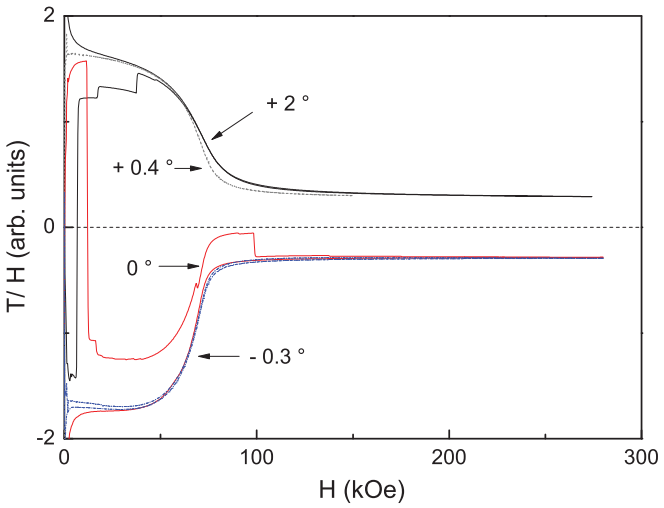

FIG. 5. (Color online) Torque signal T_x/H measured for $\mathbf{H}/H = \cos\beta\mathbf{e_z} + \sin\beta\mathbf{e_x}$ with β ranging from 2° to $-0.3°$. $\beta = 5°$ and 1° were also measured and not shown for clarity. $\beta = 6°$ is shown in Fig. 4, upper panel. $T = 300$ K.

where $\beta = 6°$ as in configuration I and η represents the misalignment of the sample when it was glued on the cantilever; using the experimental value of T_x/H at low field, one obtains $\eta = 12°$. The shape of the curve is similar to the one obtained in configuration 1, and is one order of magnitude smaller due to the misalignment coefficients. This shows that the signal is dominated by the m_c and m_a components of the magnetization, m_b being negligible as expected. In other words, configuration II demonstrates that the SR takes place in the (**a**,**c**) plane. It can be noticed that in this configuration, both m_c and m_a are positive and the signal converges to a negative value due to the negative sign of the third term. The cancellation of the experimental curve results from the compensation of the last two terms of Eq. (2) and corresponds to a tilt angle of about 20° of the weak ferromagnetic moment out of the a axis. The quality of this estimation is poorer than the previous one because of the weakness of the signal and the fitting parameter η. In configuration I, a small misalignment angle analog to η may exist, but it was neglected since it introduces $\cos\eta \approx 1$ coefficients for m_a and m_c and $\sin\eta$ for $m_b \approx 0$.

Figure 5 gathers T_x/H curves measured for different values of β. The field directions were slightly changed around the $\mathbf{e_z}$ direction (expected to coincide with the a axis of the sample) in the ($\mathbf{e_y}$,$\mathbf{e_z}$) plane. We choose $\beta = 0°$ to be the angle at which the torque switches sign.

Remarkably, the absolute value of the torque increases at the beginning of the SR for negative values of β: the angle between the directions of **m** and **H** is initially $90° - \beta$ and as the field increases up to several teslas, it decreases, going through 90° thus maximizing the torque. This indicates once again that the net magnetic moment remains in the (**a**,**c**) plane, at least at low fields.

The T_x/H signal exhibits a plateau above 200 kOe. This may come from either a finite magnetic torque or from the force applied to the sample by the field gradient due to a residual

magnetic field inhomogeneity. However, this force should be identical in our two experimental configurations, which is clearly not the case (see Fig. 4). In addition it should not change sign with β (Fig. 5). Therefore, the measured plateau results from a $\mathbf{m} \times \mathbf{H}$ term. It follows that the plateau at a finite value clearly shows that the magnetic moment and the applied field are *never* collinear for any β. Instead $\mathbf{m}$ forms a finite angle of 10° with $\mathbf{H}$. This value is of the order of the inaccuracy of the alignment of the crystallographic axes of the sample with respect to the reference system of coordinates. In order to determine if the plateau can originate from the misalignment of the sample within which $\mathbf{m}$ and $\mathbf{a}$ are collinear (Γ_2 configuration, as expected at high field), the effect of the different kinds of misalignment must be discussed; the conclusions drawn for experimental configuration I also hold for configuration II. The first type of misalignment corresponds to a rotation of the sample around the $\mathbf{z}$ direction and is represented by the angle η in Fig. 2: it leaves the a axis invariant and is thus irrelevant here. The second type arises from a rotation around the x axis and would only result in an offset in β. The third type of misalignment is a rotation around the y axis and actually introduces a constant angle offset between $\mathbf{H}$ and $\mathbf{a}$ in our experiment. This angle actually gives rise to a finite contribution to the torque but the y component of this term cannot be detected by our setup, and its x component should cancel during the β scan, when $\mathbf{H}$ belongs to the $(\mathbf{a},\mathbf{b})$ plane. In any case, the measured torque would vanish like $\sin\beta$ if the magnetic moment and $\mathbf{a}$ were collinear. We conclude that unexpectedly, $\mathbf{m}$ is tilted away from the a axis by 10°. The value of 10° agrees well with the $m_a(H_a)/m_c(H_c) = \cos 12°$ ratio obtained by VSM at 14 T. During the SR, the net magnetic moment rotates by 80° rather than 90°, and the final spin configuration is not Γ_2.

Abrupt changes of the torque signal are visible in Fig. 5. The jumps around 1 T correspond to the reversal of the ferromagnetic moment, before the SR takes place: the fields at which the torque jumps fairly follow $H_r/\sin\beta$, where H_r is of the order of 1 kOe and refers to the reversal field for the ferromagnetic moment when $\mathbf{H}$ is applied along the $\mathbf{c}$.

The curve at $\beta = 0°$ is unique. It exhibits an irreversible large jump at 100 ± 2 kOe that was observed several times: immediately after the first measurement and at the end of the β scan. However, this phenomenon takes place for a very narrow angle range $|\beta| < 0.3°$. The (quasi-) cancellation of the torque can have two relevant explanations: (i) the magnetic moment and the applied field are collinear everywhere in the sample, or (ii) the sample magnetization splits into two domains of similar volumes within which the magnetic moment is tilted by 10° away from $\mathbf{a}$. The narrow angle range for this jump to happen makes the first hypothesis quite unlikely. On the other hand, the irreversible and sharp features of the jumps match the behavior of a switch between metastable states. Figure 5 showed that there exist two possible spin configurations at the end of the SR, i.e., $\mathbf{m}$ being $+10°$ or $-10°$ away from $\mathbf{a}$ in the $(\mathbf{a},\mathbf{c})$ plane. The 100-kOe jump appears for the field direction that is the closest to the mean direction between the two final states.

We do not have enough information to determine if the small jumps at 20 and 35 kOe for $\beta = 2°, 1°$ are switches of the tilt angle rather than late ferromagnetic reversals.

IV. TWO-MACROSPIN MODEL

In the the rest of the article, we will consider the origin of the magnetic state at high field. We will first discuss whether our observations can be described by the current magnetic model or if they reveal something new.

The magnetic interactions in orthoferrites are commonly described by the following Hamiltonian:[3,9,11,12]

$$\begin{aligned}\frac{\mathcal{H}}{\mathcal{N} g\mu_B S} = &-H_E \mathbf{m_1}\cdot\mathbf{m_2} - H_D \mathbf{e_b}\cdot(\mathbf{m_1}\times\mathbf{m_2}) \\ &- \frac{1}{2}H_2\left(m_{1a}^2 + m_{2a}^2\right) \\ &+ \frac{1}{4}H_4 \sum_{\alpha=a,b,c} c_\alpha\left(m_{1\alpha}^4 + m_{2\alpha}^4\right) - \mathbf{H}\cdot(\mathbf{m_1}+\mathbf{m_2}),\end{aligned} \tag{3}$$

where g is the Lande factor; $\mathcal{N}$ is the number of Fe^{3+} ions ($S = 5/2$); H_E, H_D, H_2, and H_4 are the AFM exchange interaction, the DM interaction, and the uniaxial and cubic anisotropy interactions, respectively, expressed in field units; $\mathbf{e_{a,b,c}}$ are an orthogonal system of unit vectors based on the crystallographic axes assuming an orthogonal structure; and $\mathbf{m}_i$ are unit vectors pointing in the direction of a magnetic moment in the ith sublattice ($i = 1,2$).

A. Analytical solutions

Equilibrium states can be calculated analytically by minimizing Eq. (3) if the magnetic field is applied either along $\mathbf{e_a}$ or $\mathbf{e_c}$. In these two particular cases, the magnetic moment remains in the $(\mathbf{e_a},\mathbf{e_c})$ plane axis as confirmed by the presented experimental results. Thus, the state of the system depends on only two variables—the polar angles $\theta_{1,2}$. An additional assumption is required to obtain an analytical solution: we choose $c_x = 1$ and $c_{y,z} = 0$. By doing this, the K_4 term loses its physical meaning of cubic anisotropy contribution and becomes a phenomenological correction. The interest of introducing such an artificial parameter is that it permits a fully analytical approach that will yield all the parameters of the problem. We subsequently verified by numerical simulations that this stratagem makes no qualitative change in the observed quantities.

We introduce

$$\begin{cases}\alpha = \frac{1}{2}(\theta_1 + \theta_2 - \pi) \\ \phi = \frac{1}{2}(\theta_1 - \theta_2 + \pi),\end{cases} \tag{4}$$

where θ_i are the polar coordinates of $\mathbf{m}_i$ on the unit sphere. α represents the angle of AFM with respect to $\mathbf{e}_a$ and ϕ is the canting angle of the two sublattices with respect to the AFM axis, respectively. Then, the net magnetization $\mathbf{M} = \mathcal{N} g\mu_B S(\mathbf{m}_1 + \mathbf{m}_2)$ in the particular cases $\mathbf{H} = H\mathbf{e_a}$ and $\mathbf{H} = H\mathbf{e_c}$ is, respectively,

$$M_a(H) = \mathcal{N} g\mu_B S \sin\phi \sin\alpha, \tag{5}$$

$$M_c(H) = \mathcal{N} g\mu_B S \sin\phi. \tag{6}$$

The H dependence of ϕ and α is obtained by minimization of Eq. (3) as proposed by Jacobs *et al.*,

$$\sin\phi = \frac{H_D + H}{2H_E}, \forall H, \tag{7}$$

and

$$\begin{cases} (2H_2H_E - 4H_4H_E - H^2)\sin\alpha & \\ +4H_4H_E\sin^3\alpha - H_DH & = \quad 0, H < H_0 \\ \sin\alpha & = \quad 0, H > H_0. \end{cases} \tag{8}$$

Finally, the reorientation field H_0 is given by

$$H_0 = \frac{-H_D + \sqrt{H_D^2 + 8H_2H_E}}{2}. \tag{9}$$

B. Physical parameters

The zero-field canting angle ϕ_0 can be evaluated from the experimental zero-field magnetization M_0 by Eq. (6). The obtained value of ϕ_0 in Eq. (7) for $H = 0$ yields the H_D/H_E ratio. For $H > 0$, the magnetization is described by $M_c(H) = M_0 + \chi H$ where the slope χ is the transverse AFM susceptibility. By identification of χ in Eqs. (6) and (7), we get H_E and thereby, H_D. Introducing them into Eq. (9) gives H_2. Finally, H_4 is fitted to the experimental magnetization for $\mathbf{H} = H\mathbf{e_a}$ ($H < H_0$) using the previous parameters. The agreement with experimental data is illustrated by numerical solutions (Fig. 3), which are identical to the analytical ones. The parameters are summarized in Table I for $T = 4.2$ and 300 K; parameters from Ref. 9 are also given for comparison.

C. Numerical simulations

The numerical minimization of Eq. (3) were calculated by a relaxation method. The time dependence of our system is ruled by the Landau-Lifshitz-Gilbert equation,

$$\frac{\partial\mathbf{m}}{\partial t} = -\mathbf{m}\times\frac{\partial\mathcal{H}}{\partial\mathbf{m}} - \varepsilon\left(\mathbf{m}\times\frac{\partial\mathbf{m}}{\partial t}\right), \tag{10}$$

where ε is the damping parameter and is considered an arbitrary computational parameter. Equation (10) can be rewritten as

$$(1+\varepsilon^2)\frac{\partial\mathbf{m}}{\partial t} = -\mathbf{m}\times\frac{\partial\mathcal{H}}{\partial\mathbf{m}} + \varepsilon\,\mathbf{m}\times\left(\mathbf{m}\times\frac{\partial\mathcal{H}}{\partial\mathbf{m}}\right). \tag{11}$$

The solutions of Eq. (11) converge toward the equilibrium state. The validity of the program was established by reproducing the analytical solutions (for **H** applied along **a** and **c**) with excellent agreement.

V. DISCUSSION

The equilibrium magnetization curves calculated for $\mathbf{H}\|\mathbf{a}$ and $\mathbf{H}\|\mathbf{c}$ are plotted with the experimental data in Fig. 3. In contradiction with the experimental results, the two curves are identical at high field. This means that the magnetic interactions involved in the model of Eq. (3) yields a SR from Γ_4 at low field to Γ_2 above H_0. The simulations also confirm that the misalignment is not responsible for the plateau at a finite value in the torque signal. The magnetic torque was computed for the experimental conditions, i.e., including the misalignment angle $\eta = 12^\circ$: the applied magnetic field expressed $\mathbf{H} = \cos\beta\mathbf{e_z} + \sin\beta\mathbf{e_y}$ in the reference system of coordinates corresponds to $\mathbf{H} = \cos\beta\mathbf{e_a} - \cos\eta\sin\beta\mathbf{e_b} + \sin\eta\sin\beta\mathbf{e_c}$ (with $\beta = 6^\circ$) relative to the sample crystallographic directions. The simulations are presented in Fig. 4 for configurations I and II. Similar to the magnetization, the theoretical calculations agree very well with the experiment during the SR, but fail to reproduce the final state. In both configurations, the calculated final states are essentially Γ_2. This leads to the overestimation (underestimation) of m_a (m_c) in Eqs. (1) and (2).

To explain the failure of the model to describe the magnetic state after the SR, one may consider an extra interaction that would not have been taken into account yet and whose effect can only be observed at high field. First, we introduced anisotropic exchange as suggested in Ref. 11. We did include anisotropic exchange either along the a axis or along the c axis into the Hamiltonian expression and systematically varied its reduced intensity from 10^{-5} to 10^{-2}, with both signs. Second, we considered the effect of a more realistic DM interaction by taking into account four sublattices instead of only two. We used the model proposed by Herrmann[13] that includes six Dzyaloshinsky-Moriya vectors corresponding to the antisymmetric exchange coupling of each pair of sublattices and using combinations of reduced values ranging from $0.01h_D$ to $100h_D$. The calculation code was validated by the analytical solution as was previously done, using parameters matching the two-sublattice case. Third, we arbitrarily introduced a sixth-order anisotropy term $\mathcal{H}_6 = -1/6H_6(m_{x1}^6 + m_{x2}^6)$, with H_6/H_e ranging from $0.01h_2$ to $100h_2$. None of these three attempts could account for the incompleteness of the spin reorientation. For the sake of clarity, only the simplest model is presented.

The discrepancy between theory and experiment can be ascribed to a modification of the magnetic interactions during the SR. Structural changes, possibly associated with a symmetry change induced by magnetostriction, are likely to happen with the SR. Given the very high anisotropy of the magnetic interactions, the rotation of the magnetization induces a strain on the ionic lattice. This strain has been evidenced through the macroscopic expansion of the samples ($YFeO_3$[14] and $ErFeO_3$[7]), but no information on the consequences of the strain on the crystallographic order have been published so far. The field-induced SR at a fixed temperature was studied by neutron diffraction by Koehler *et al.* on $ErFeO_3$ and $HoFeO_3$ up to 10 kOe.[10] Their results suggest structural domain transformations during the SR but many details were lost since they studied powders and they considered the structure as cubic to interpret the magnetic ordering. This hypothesis of a change of the magnetic interactions subsequent to a symmetry change of the crystal is coherent with the excellent agreement of the model at low field and its failure after the SR.

Independent of its origin, the high-field magnetic state is noteworthy. The a axis appears as a forbidden direction for the magnetization, whose direction remains tilted by 10° away from the a axis. This raises the question of the potential barrier separating the two metastable states.

VI. CONCLUSION

We reported results on the magnetic-field-induced SR in single crystals of yttrium orthoferrite. By means of a torque magnetometer under high magnetic field we showed that the magnetic state is not Γ_2 as predicted by theoretical models. Instead of rotating by 90° under the effect of the applied field, the magnetic moment only rotates by 80°, thus pointing about 10° out of a crystallographic axis. These results point at the limitation of the description of the magnetic interactions that have been considered so far in orthoferrites. However, the success of the existing model at low field suggests that its failure at high field reveals a change of the symmetry of $YFeO_3$ during the SR.

ACKNOWLEDGMENTS

We acknowledge the Transnational Access–Contrat n° 228043–Euromagnet II–Integrated Activities of the European Commission for granting the high-field experiments. This work was supported by the region Ile-de-France, C'Nano NOVATECS Project No. N°IF-08-1453/R. We thank the Centre de Ressources Informatiques de Haute-Normandie (CRIHAN) for the use of its computing resources.

[1] I. Dzyaloshinsky, J. Phys. Chem. Solids **4**, 241 (1958).
[2] T. Moriya, Phys. Rev. **120**, 91 (1960).
[3] D. Treves, Phys. Rev. **125**, 1843 (1962).
[4] R. L. White, J. Appl. Phys. **40**, 1061 (1969).
[5] L. T. Tsymbal, V. I. Kamenev, Y. B. Bazaliy, D. A. Khara, and P. E. Wigen, Phys. Rev. B **72**, 052413 (2005).
[6] Y. B. Bazaliy, L. T. Tsymbal, G. N. Kakazei, V. I. Kamenev, and P. E. Wigen, Phys. Rev. B **72**, 174403 (2005).
[7] R. P. Chaudhury, B. Lorenz, C. W. Chu, Y. B. Bazaliy, and L. T. Tsymbal, J. Phys. Conference Series **150**, 042014 (2009).
[8] J. Scola, W. Noun, E. Popova, A. Fouchet, Y. Dumont, N. Keller, P. Lejay, I. Sheikin, A. Demuer, and A. Pautrat, Phys. Rev. B **81**, 174409 (2010).
[9] I. S. Jacobs, H. F. Burne, and L. M. Levinson, J. Appl. Phys. **42**, 1631 (1971).
[10] W. C. Koehler, E. O. Wollan, and M. K. Wilkinson, Phys. Rev. **118**, 58 (1960).
[11] C. W. Fairall and J. A. Cowen, Phys. Rev. B **2**, 4636 (1970).
[12] G. Gorodetsky, S. Shtrikman, Y. Tenenbaum, and D. Treves, Phys. Rev. **181**, 823 (1969).
[13] G. F. Herrmann, Phys. Rev. **133**, A1334 (1964).
[14] A. M. Kadomtseva, A. P. Agafonov, M. M. Lukina, V. N. Milov, A. S. Moskvin, V. A. Semenov, and E. V. Sinitsyn, Zh. Eksp. Teor. Fiz. **81**, 700 (1981) [Sov. Phys. JETP **54**, 374 (1981)].